Development of a Micromachining Centre and Fabrication and Characterization of Watchmaking Parts

Gonçalo de Almeida Domingos
goncalo.almeida.domingos@gmail.com
Instituto Superior Técnico, Universidade de Lisboa, Portugal

October 2020

Abstract: In mechanical watchmaking, time is measured through the use of an oscillator, composed of the balance wheel and balance staff, whose pivots run on a pair of jeweled bearings. These pivots have characteristic dimensions of around 100 μm, must possess high hardness ($\sim$ 50 HRC), a very fine surface finish ($R_a \sim 0.1\ \mu m$) and high dimensional accuracy on the diameter (+0 /-3 μm). The goal of this thesis was to improve an existing 5 axis machining centre with a modern CNC controller and a specific electro-mechanical framework for watchmaking research. The first part of this thesis focused on the improvements made to the machining centre, both on its mechanical and metrological front and on the application of a new electronic and control structure. Following these improvements, to simulate the manufacture of the pivots, a series of micro-turning trials were conducted by turning small diameter (between 300 and 100 micron) micro-pins. The trials were designed so that the effect of the operating parameters, depth of cut, feed rate and the presence of lubricant, on the surface finish and dimensional accuracy of the micro-pins could be studied. The results obtained show that the dimensional accuracy is substantially influenced by the metrological characteristics of the machine and the surface finish by the operating parameters, with best results ($R_a = 0.240\ \mu m$) obtained without lubricant and low depths of cut and feed rates.

Keywords: watchmaking, micro-turning, surface finish, R_a, CNC.

1. Introduction

Arguably, one of the defining inventions in watchmaking history was the *balance spring*, developed around the 1650s and credited to both Huygens and Hooke, which consists in a finely coiled, hair thin spring which, when connected to the *balance wheel* (fig.1), increased its time regulating characteristics. The interaction between the balance wheel and the balance spring effectively turns them into an harmonic oscillator, with a precisely defined oscillating period T (s), dependant on both the balance wheel inertia I ($kg{\cdot}m^2$) and the balance spring stiffness k $\left(\frac{N \cdot m}{\text{rad.}}\right)$ through eq.1.

$$T = 2\pi \left(\sqrt{\frac{I}{k}}\right) \tag{1}$$

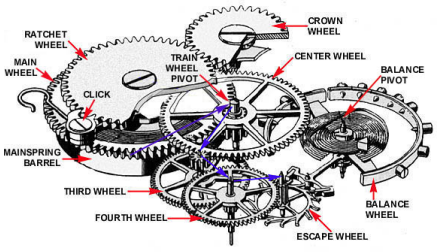

Figure 1: A conventional mechanical watch gear train [1]

The effectiveness of a watch as a timekeeper is however not only dependent on the balance wheel. Ideally, this oscillator would remain undisturbed throughout its oscillating cycle, which would ensure that the time taken during one oscillation would remain constant (a characteristic called *isochronism*). However, the balance wheel runs in a cylindrical shaft, called the *balance staff*, with two fine pivots, *balance pivots*, running on a pair of bearings, which contribute to most of its energy dissipation, due to the continuous oscillation and the high frequency stop and start motion. A significant improvement, directly targeted at decreasing this loss of energy and improving timekeeping, was the introduction of jeweled bearings.

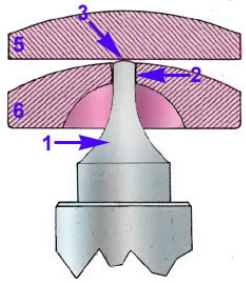

Figure 2: A watch balance staff pivot running on jeweled bearings [1]

First adapted for use in balance staff pivots, referring to fig.2, the conical pivot ① was constrained ax-

ially (vertical in the figure) by running its *seat* ③ on the *endstone* ⑤. The radial (horizontal in the figure) constrain was accomplished by running the pivot main bearing surface ② against the *pierced jewel* ⑥. Their advantages reside in their extreme hardness, their dissimilar nature to the metal pivot and the ease of reaching near perfect polishes on the running surface (R_a = 0.025 to 0.05 μm). All these characteristics decrease wear and, due to the extremely fine finish achievable, the achievable coefficient of friction of steel on sapphire is 0.1 - 0.15 [2].

The purpose of this work is to redesign an existing turning machine, with an improved kinematic chain, a modern CNC controller and a specific electromechanical framework, and use it to manufacture several micro-pins with diameter ranging from 300 down to 100 μm through micro-turning operations, as a demonstrator of the machine capability to produce parts similar to balance staff pivots and others relevant for watchmaking research. These pins will further be characterized regarding their dimensional accuracy on the diameter and their surface finish in the form of the parameter R_a, resulting from the metrological characteristics of the redesigned machine and the operational parameters during the micro-turning operations.

2. Machine introduction

The Proteo machine (fig. 3) was originally designed as small envelope machining centre, capable of realizing synchronized movements in four simultaneous axis.

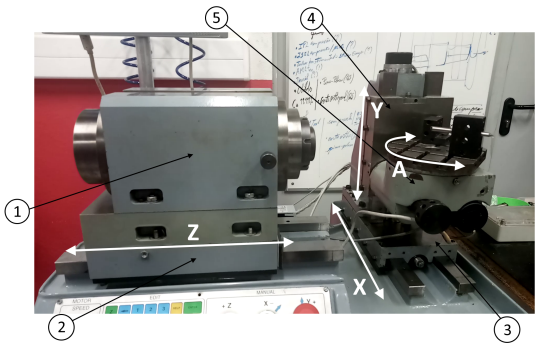

Figure 3: The Proteo machining centre

2.1. Mechanical assessment and improvement

The existing machining centre required several mechanical improvements to bring it to working condition. The most significant problems were the bow and wear of the guideways (master rail), the wear of the preload gibs due to contact with the master rail and the lack of a manual drawbar mechanism.

2.1.1. Linear axes: grinding the master rails

The hardened steel master rails had significant side wear due to years of operation without proper lubrication and maintenance, and excessive and uneven preload.

The grinding operation was performed (fig. 4) until sparking could be observed all across the surface of the master rail. This meant the entire surface was flat. The result were two master rails with as close to parallel ($\approx$ 10 μm over 400 mm) sides as the author could accomplish, given the state of the grinder and his operating experience.

2.1.2. Linear axes: production of preload gibs

The existing cast iron gibs, due to the incorrect preload adjustment through the linear axes side screws, coupled with with the high wear, were severely warped. It was therefore necessary to produce new ones. In an attempt to alleviate the wear problem in the future, brass was used instead of cast iron (bronze, although ideal, was not readily available in bar stock form in the workshop). It has better sliding properties against hardened steel, comparable stiffness and machines readily. The gibs were produced on a conventional milling machine (fig. 5).

2.1.3. Headstock: production of drawbar

The original headstock used a pneumatic drawbar mechanism to actuate the opening and closing of the collets. The pneumatic closing assembly however was incomplete, and therefore an adaption of the existing drawbar was made so that manual closing could be used instead. Fabrication of the parts to accomplish the same function was quite straightforward.

A spacing ring in aluminium was turned and, to be able to thread the drawbar into the collet, an aluminium disk was also face turned to act as a handwheel. It was followed by drilling and boring of a pilot hole in its center. Finally, the pilot hole was threaded M20x1.5, the available thread in the drawbar (see fig. 6 for complete drawbar).

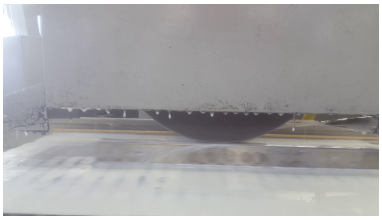

Figure 4: Grinding the master rail

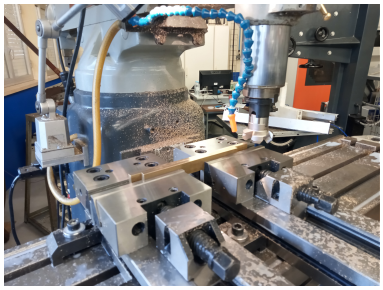

Figure 5: Making of the brass gibs

Figure 6: Completed drawbar.

2.2. Electronic framework improvement

What initially prompted the retrofit work was the failing electronic framework of the Proteo machine. Therefore a brand new and specific control and electronic system was applied to the machine.

2.2.1. Servo amplifiers

Four servo amplifiers from CNCDrive were acquired. These are simple, DC brushed servo motor amplifiers, with quadrature encoder input, and purely positional control.

2.2.2. CNC controller

A LinuxCNC solution was selected based on total cost, with hardware from MESA (6i25 and 7i76).

2.2.3. Upgrade of rotary encoder of the X axis

Upon assembly of the servo amplifiers, it was necessary to perform tuning of the linear and rotary guideways. It was at this point that the resolution limit of the original encoders was made apparent. An eight times higher count encoder (CUI AMT 102) was tested in the x-axis, which produced a much smoother motion.

2.2.4. Spindle: DC drive

A modern DC drive from Parker (SSD 506) was acquired since the original electronics were highly integrated and no salvage was possible.

3. Experimental methodology

3.1. Performance criteria

Balance staves manufactured today, using state of the art machining techniques and machines, satisfy strict design criteria to ensure proper operation over their lifetime. An adaptation of these criteria was made to be able to realize the necessary trials and measurements, and the following performance criteria were established:

- Simplified geometry: simple cylindrical pin with a diameter of around 300 μm, length of approximately 4mm; tight control over diameter (h4 tolerance - +0/-3μm [3]);
- Surface roughness values of at most 0.4 μm R_a, ideally closer to 0.1 μm [2];
- Free cutting material: brass (CuZn39Pb3);

3.2. Trial conditions

In order to check the dependence of both the surface roughness and diameter figures, several trials were conducted, over a region (table 1) which encompassed different combinations of depths of cut (a_p) and feed rates (f), limited by the manufacturer recommendation for the cutting tool (Palbit DCGT070202-LN PH0910).

	a_p *(mm)*					
	0.5	0.9	1.3	1.7	2.1	2.5
0.005	x	x	x	x	x	x
0.010	x	x	x	x	x	x
0.020	x	x	x	x	x	x
0.040	x	x	x	x	x	x
0.080	x	x	x	x	x	x
0.160	x	x	x	x	x	x
f (mm/rev.)						

Table 1: Trial map

Since the intention was to fabricate micro-pins, a single cutting pass was executed over the length of the micro-pin, in order to minimize the deflection and avoid deformation due to excessive forces generated in relation to the micro-pin cross section.

3.3. Measurements

Force measurements were made using a piezoelectric load cell from Kistler (typ. 9121), using a charge amplifier and a DAQ from NI (USB-6001), all captured in LAbView. Surface roughness measurements were taken three times on each trial in three different positions, with a Mahr M300. Diameters were measured using a micrometer

4. Results

4.1. Metrological characterization of the machine

After assembly of the machine, and prior to the micro-pin trials, a simple metrological assessment of the machine was made. Tests were performed to check for squareness between the X and Z axes (orthogonality), the positional accuracy of the X axis and the runout (difference between the axis of rotation of the workpiece and the main axis of rotation) of the spindle.

4.1.1. Squareness error

After assembling the headstock, alignment was performed to decrease coupling errors between the X and Z axis. By careful alignment, the final error measured to be 35 μm over 35 mm of travel. Over the length of the micro-pin, 4 mm, this meant a difference of around 4 μm, sufficiently low given the magnitude of other errors.

4.1.2. Accuracy of the X axis

Since the critical dimension of the micro-pins was their diameter, the X axis of the machine was tested to check for unidirectional accuracy. By commanding the X axis to move with similar step sizes R_a to those of table 1, the actual measured movement with the dial indicator was averaged over 30 measurements (μ), and the difference $\delta a_p = a_p - \mu$, the undershoot, was calculated and is presented below, as is its standard deviation, σ.

- a_p = 0.5 mm: δa_p = 0.021 mm, σ = 0.009 mm;
- a_p = 0.9 mm: δa_p = 0.016 mm, σ = 0.004 mm;
- a_p = 1.3 mm: δa_p = 0.013 mm, σ = 0.004 mm;
- a_p = 1.7 mm: δa_p = 0.013 mm, σ = 0.003 mm;
- a_p = 2.1 mm: δa_p = 0.011 mm, σ = 0.003 mm;
- a_p = 2.5 mm: δa_p = 0.010 mm, σ = 0.002 mm;

4.1.3. Runout error

The measured runout was 20 μm at a projected length of 5 mm. No adjustment could be performed to decrease this error.

4.2. Machining trials: Overall view

Trials were conducted within the operating map defined in table 1. In the following sections, cells marked with a cross were trials where either micro-pins could not be fabricated or where no trials were conducted based on previous results.

4.2.1. Machining trials: Diameter

The first trials were conducted for 300 μm micro-pins, with corresponding diameters in table 2.

	a_p (mm)					
	0.5	0.9	1.3	1.7	2.1	2.5
0.005	324	320	314	309	297	295
0.010	320	325	318	309	295	276
0.020	328	325	322	305	285	275
0.040	330	336	326	327	x	x
0.080	366	371	415	x	x	x
0.160	x	379	x	x	x	x
f (mm/rev.)						

Table 2: Measured diameters (μm) for the various fabricated micro-pins (300 μm trials)

Other trials were realized for lower diameter micro-pins (with corresponding measured diameters in table 3 for 150 and 100 μm trials).

	a_p (mm)			
	0.5	0.9	0.5	0.9
0.005	155	177	117	128
0.010	161	165	109	123
	(150 μm)		*(100 μm)*	
f (mm/rev.)				

Table 3: Measured diameters (μm) (150 and 100 μm trials)

Measured values for 150 and 100 μm trials are within the maximum acceptable diameter, calculated taking into account both deflection and undershoot (accuracy of the X axis). However, in the 300 μm trials, measured diameters at f = 0.080 and a_p = 0.9 and 1.3, and at f = 0.160 mm/rev. are higher than the maximum acceptable, while at a_p = 2.1 and 2.5 they are below the targeted diameter. The difference between the measured and calculated maximum acceptable diameters are thought to be due to three phenomena:

(i) Coupling effects: Although the dynamometer, which is itself the tool holder, is extremely rigid (600N/μm), its connection to the X axis guide is mechanically poor (fig. 7, circled in red, two bolts providing hold down torque, but no pinned joint or register to locate it), which means that it has low stiffness. Further, a long *structural loop* (fig. 7, yellow dashed line) exists between the tool and the spindle, which contributes to the overall low stiffness of the machine.

Simultaneously, when the tool is fed into the workpiece, its *interaction area* is dependent on two factors, f and a_p. An increase in $A_{int.}$ leads to a better cou-

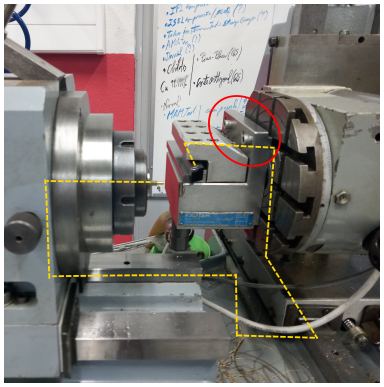

Figure 7: Tool holder mechanical connection and structural loop

pling between the forces exerted during machining trials and the dynamometer - X axis guide interface (and the whole machine). This improved coupling effectively transfers part of the forces experienced during machining to actuate this interface, which generates vibrations of the tool in all directions. The result of this is that the tool center position is not exactly determined and as a consequence the diameters of the micro-pins are not as tightly controlled.

(ii) Tool center height: The tool center height affects the true turned diameter. Due to the small diameter of the micro-pin, it was not easy to adjust nor measure the vertical offset from the ideal position, although it was optically verified that the tool was below centre (fig. 8).

(iii) Error in measurement: Particularly for the six trials (at a_p = 2.1 and 2.5 mm) where the measured diameter is below 300 μm, the only possibility is that during the first operation to determine the zero of the tool, the incorrect diameter was taken with the micrometer.

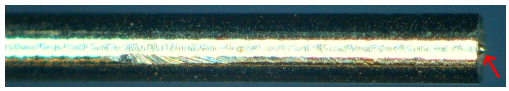

Figure 8: Tool center height misalignment: small "nipple" at the end of the micro-pin

4.3. Machining trials: Surface roughness R_a

Over the whole map (table 4), R_a increases with increasing a_p and f. While the dependence on f was expected (and seen in figs. 9 and 10), on the contrary, the dependence on a_p was not. R_a, which is given by

$$Ra_{theo.} = \frac{f^2}{32 r_b} \tag{2}$$

where r_b is the *tool nose radius*, suggests no such dependence.

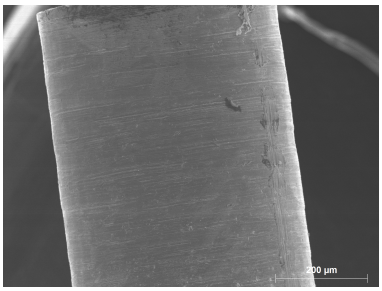

Figure 9: SEM micrograph of micro-pin at const. a_p = 1.7 mm and low f (0.005 mm/rev.)

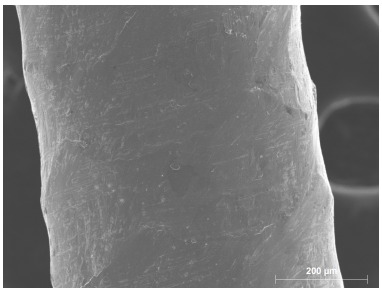

Figure 10: SEM micrograph of micro-pin at a_p = 1.7 mm and high f (0.040 mm/rev.)

The following hypothesis were proposed: **(i)** same as hypothesis 1 of section 4.2.1. Recalling it, since the tool center point is affected by the vibration, which is increased by an increase in $A_{int.}$, then we assume that

$$Ra_{vib.} = f(A_{interaction}) \tag{3}$$

The increase of $A_{int.}$ along varying a_p and fixed f is different from its increase along varying f and fixed a_p. After some calculations,

$$A_{interaction} \propto \begin{cases} a_p^2 + a_p d & \text{if at const. } f \\ f & \text{if at const. } a_p \text{ and large } f \end{cases} \tag{4}$$

Under this hypothesis, eq.2 can be changed to

$$Ra_{exp} = Ra_{vib.}(a_p, f) \tag{5}$$

where the theoretical term was dropped since a_p and large f are no longer well defined due to vibration. (the exact dependence of $R_{avib.}$ is not taken as ${a_p}^2$, a_p and f since the exact function in eq. 3 is unknown).

(ii) finite stiffness of micro-pins. The deflection Δy the micro-pins are subjected to is

$$\Delta y = \frac{128 F_y L^3}{6 E \pi D^4} \tag{6}$$

	a_p (mm)					
	0.5	0.9	1.3	1.7	2.1	2.5
0.005	0.280	0.252	0.310	0.340	0.944	2.099
0.010	0.268	0.240	0.374	0.591	1.901	3.056
0.020	0.485	0.485	0.761	1.373	4.051	4.266
0.040	0.808	1.053	1.600	3.364	x	x
0.080	2.069	2.077	2.121	x	x	x
0.160	x	3.797	x	x	x	x
f (mm/rev.)						

Table 4: Surface roughness R_a (μm) of the various micro-pins. Cells marked at grey meet the performance criteria for R_a ($< 0.4\ \mu m$)

where *L* is the length of the overhanging pin (a function of the axial position of the tool), and *D* is its initial diameter, a function of a_p: $D = 0.3 + 2a_p\ (mm)$.

The dependence on *L* is constant, since all pins have roughly the same length. While at the beginning of the trial the pin is at its most overhang, the actual a_p is not the expected, since the tool might not even be engaging the pin properly, instead sliding along the surface, potentially causing severe rubbing and adhesive wear and increasing R_a. By the end of the trial, the pin is at its lowest overhang, and this effect is less noticeable (example of this effect in fig. 11). Also, trials conducted at smaller pin initial diameter will suffer higher deflections that those with larger diameters. This is equivalent to saying

$$\Delta y \propto \frac{1}{D^4} \propto \frac{1}{a_p^4} \tag{7}$$

Under this hypothesis

$$Ra_{defl.} = f(\Delta y) \tag{8}$$

Therefore, under these two hypothesis, a modified eq. 2 is proposed

$$Ra_{exp} = Ra_{vib.}(a_p, f) + Ra_{defl.}(a_p) \tag{9}$$

(again the exact dependence of $R_{adefl.}$ is not taken as a_p^{-4} since the exact function in eq. 8 is unknown).

with each term having the following general behaviour:

$$Ra_{vib.}(a_p, f) \begin{cases} \uparrow\uparrow \text{ as } a_p \uparrow \\ \uparrow \text{ as } f \uparrow \end{cases} \tag{10}$$

$$Ra_{deflection} \downarrow \text{ as } a_p \uparrow \tag{11}$$

Therefore, according to this two hypothesis, **a_p should be a stronger estimator of R_a than f**.

A competition between these two potential mechanisms occurs: in the region where a_p is small (0.5 - 0.9 mm), the deflection term $Ra_{defl.}$ appears to dominate at low values of f (0.005 - 0.010 mm/rev.). Crossing from a_p = 0.5 mm to 0.9 mm, a reduction of R_a occurs due to an increase of the pin initial diameter, which lowers deflection and therefore lowers the contribution of $Ra_{defl.}$ towards the total Ra value. Contrary to the expected, from f = 0.005 mm/rev. to 0.010 mm/rev. R_a decreases. The difference between values is small enough that their difference can be merely statistical in nature, due to the small population of samples;

A transition at f (0.020 mm) to a zone where the vibration term $Ra_{vib.}$ takes over can be seen f (0.040 - 0.160 mm), since if the main contributor to R_a here was $Ra_{defl.}$, the total R_a value should be constant along the constant a_p (vertical) lines.

Independently of f, beyond a_p = 1.3 mm, the effect of $Ra_{vib.}$ overwhelms $Ra_{defl.}$.

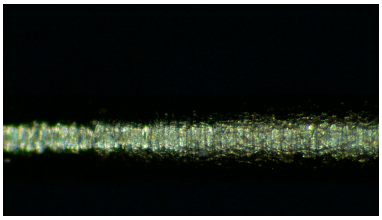

Figure 11: The effect of deflection on R_a

4.4. Machining trials: Surface roughness R_a with lubricant

Given the performance criteria established in section 3.1, it is possible to select an optimal operating zone where both diameter and R_a are within spec, which corresponds to the low-mid a_p (ranging from 0.5 to 1.7 mm) and low f (ranging from 0.005 to 0.010 mm/rev.) (excepting the value at a_p = 1.7 mm and f = 0.010 mm/rev., which was included for completeness), marked in table 4 with grey cells. Further trials were realized in this zone to check if the introduction of ***lubricant*** during micro-turning would bring a reduction of R_a to $< 0.1\ \mu m$ (table 5).

Contrary to what was expected, an increase in R_a

	a_p (mm)			
	0.5	0.9	1.3	1.7
0.005	0.378	0.358	0.510	0.594
0.010	0.420	0.300	0.646	0.763
f (mm/rev.)				

Table 5: Surface roughness R_a (μm) of the various micro-pins machined with lubricant. Cells marked at grey meet the performance criteria for R_a ($< 0.4\ \mu m$)

was verified.

4.5. Machining trials: Optimal operating zone model

To evaluate the influence of the main factors and possible interactions between a_p, f and the presence of lubricant on R_a, a full factorial, 3 factor model was generated in a DOE software, with the following parameters:

- Factor A: a_p - 4 levels (0.5, 0.9, 1.3 and 1.7 mm)
- Factor B: f - 2 levels (0.005 and 0.010 mm/rev.)
- Factor C: Lubricant - 2 levels (yes and no)

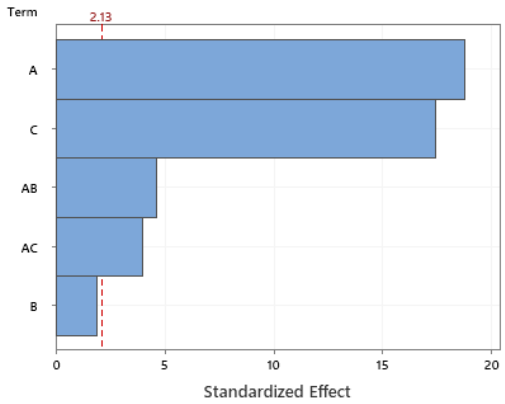

Figure 12: Pareto chart

4.5.1. Strongest predictor: a_p

The results show (A in fig. 12) that the strongest predictor of R_a is a_p. The previously put forward hypothesis also generated such a dependence.

4.5.2. Second strongest predictor: Lubricant

The second most significant predictor of R_a is the ***lubricant*** (C in fig. 12). Noticed during every trial with lubricant was that due to the *viscosity* of the cutting fluid, chips could not be evacuated from the cutting zone at all, and accumulated along the cutting front and on the backside of the cutting tool, the region of the newly formed micro-pin. This, combined with the long *residence time* of the tool in the cutting area due to low f, increases the likelihood of chip contact with the micro-pin, in turn causing rubbing and increasing R_a.

4.5.3. Predictor interactions: a_p and f

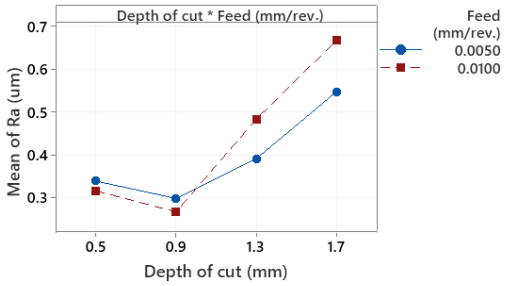

Figure 13: Interaction effects between a_p and f

First, the effect of a_p is compounded by the increase in f (seen in fig.13). In the low a_p zone (0.5 - 0.9 mm), the effect of $Ra_{deflection}$ dominates over $Ra_{vib.}$. It decreases in strength as a_p increases (as expected), and the interaction between a_p and f, seen by the close parallel lines of different f, is almost nonexistent, consistent with the hypothesis that $Ra_{deflection}$ is not a function of f.
On the contrary, after the transition from $a_p = 0.9$ mm to 1.3 mm and larger, where $Ra_{vib.}$ starts to dominate, the lines are also parallel, but are much farther apart. This means that at high enough a_p, this parameter has an influence on how strong the effect of f is (a_p uplifts f). This indicates that the particular relationship between $Ra_{vib.}$ and f is dependent both on a_p and f (through $a_p f$, according to this model).

4.5.4. Predictor interactions: a_p and presence of lubricant

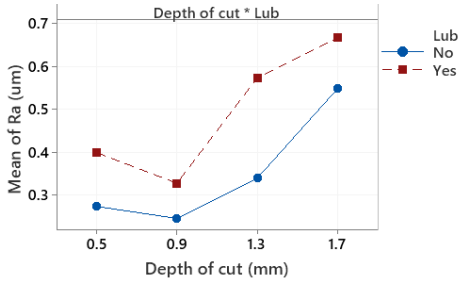

Figure 14: Interaction effects between a_p and *lubricant*

The effect of a_p is also compounded by the application of lubricant (seen in fig. 14), although the effect is subtle, making it hard to extract any useful explanation to what is in fact happening. In this figure,

the distance between the lines corresponding to trials without and with lubricant varies with a_p (highest at a_p = 1.3 mm, lowest at 0.9 mm and similar at 0.5 and 1.7 mm). If the effect was that the accumulation of the metal chips caused more contact between them and the surface of the micro-pin due to an increase in vibration, then the lines should diverge for increasing a_p. If this was not the case, and instead the effect was that the metal chips merely accumulated in the newly formed micro-pin zone, then no increase with a_p should be seen, and both lines should be parallel. More trials should be conducted to try and find the real mechanism behind this interaction.

4.5.5. The case of *f*

From the data available, it is not possible to conclude that *f* is an effective predictor of R_a by itself (B in fig. 12). Under the developed hypothesis, R_a is assumed to be a function of the interaction area which, is roughly independent of *f*, if this factor is low enough. This is a strong indication that the hypothesis put forward might be correct.

4.6. An overview of forces generated in the optimal operating zone

While not the main concern of this work, a brief discussion of the measured cutting forces in terms of the *specific cutting force* k_s $\left(\frac{N}{mm^2}\right)$ (in table 6) will be made.

	k_s $\left(\frac{N}{mm^2}\right)$	
	Dry	Lubricated
0.005	1571	1325 (- 15.6%)
0.010	1219	1082 (- 11.2%)
f (mm/rev.)		

Table 6: Specific cutting force results

The following can be stated then: that the increase in *f* decreases k_s, while the presence of lubricant also decreases this parameter. While no explicit dependence of k_s on material and process parameters was introduced, this factor is a reflection of the energy balance in the turning process, which, according to [4] is (in a simplified way)

$$dU_{ext} = dU_c + dU_f + dU_d(+dU_{fw}) \qquad (12)$$

where, during a movement of the tool dx in fig. 15, these terms can be expressed as: $dU_{ext} = F_c dx$ is the supplied energy, $dU_c = G_c b dx$ is the fracture energy (and G_c the *fracture toughness*) necessary to initiate fracture and create new surfaces, $dU_f = S dx$ is the friction dissipated energy (and S the *shear force*) and dU_d is the energy used in plastically deforming the material. The term under parenthesis, dU_{fw}, is not present in [4] but should also be considered, the friction between the tool and the workpiece.

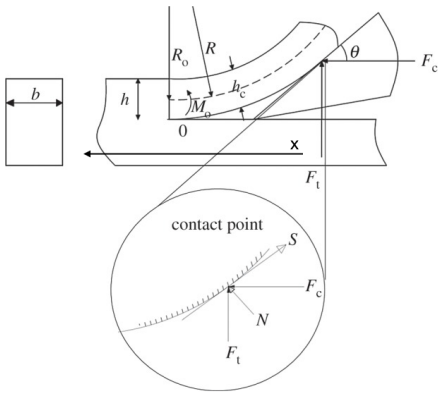

Figure 15: Interaction between tool and forming metal chip [4]

The observed reduction of k_s with the introduction of lubricant can be seen as a reduction of the friction energy dU_f and dU_{fw}, dissipated at the tool-chip and tool-workpiece interfaces respectively, while both dU_d and dU_c remain constant, since the amount of material being removed is the same. The reason why k_s decreases with the increase in *f* is three-fold, due the relative importance of the terms in eq. 12. First, at the highest *f*, the ratio between new surface area created and deformed volume of material is lower than at low *f*, since higher *f* equates to higher initial chip thickness *h* (fig. 15). In other words, at a lower *f*, more surface area has to be created per unit of deformed material than at a higher *f*, leading to higher k_s through an increase of dU_c. Second, this increased ratio between surface area and deformed volume at lower *f* means that chips are thinner, and therefore, to remove the same volume of material more chips have to flow across the cutting edge of the tool, increasing dU_f. Finally, at lower *f*, the residence time of the cutting tool in the cutting zone is greater, which increases the friction work dU_{fw}. All these mechanisms are responsible for the different relative reduction of k_s (15.6% vs. 11.2%). Clearly, both friction at the tool-chip and tool-workpiece interfaces and fracture of the material are important mechanisms in metal cutting, since k_s is significantly higher than the yield strength of brass ($\sigma_Y = 200$ MPa $Rp_{0.2}$).

4.7. Relationship between cutting force and R_a

The results show that although optimal R_a values are obtained in a low F_c zone, the best R_a is not obtained at the lowest F_c, both in dry and lubricated

regimes. This follows from the previous analysis as well as from the hypothesis regarding the dependence of R_a on a_p and f. The lowest F_c are obtained at a_p = 0.5 mm, which is the region where deflection is largest (recall eq.7), and therefore, according to the hypothesis in eq.11, R_a is degraded. This also means, under the developed hypothesis, that the true a_p is lower than 0.5 mm. On the other hand, in light of the previous analysis of F_c, since a_p is lower than the expected, the chip thickness b in fig. 15 is lower, which in turn decreases the contribution of dU_c to dU_{ext}, or equivalently, decreases F_c.

5. Discussion and conclusions

5.1. Diameter

One of the performance criteria was that the diameter tolerance should be h4, a typical precision tolerance for shaft running on a precision plain contact bearing. This is because a tolerance of h4 (+0/-3 μm for the fabricated micro-pins, independent of diameter), given a positive tolerance of H6 (+5/-0 μm) for the jewel, assures a 7 ° maximum lean of the balance staff in its jewel, the ideal case according to [3]. Clearly, the results are far from what is necessary for the correct functioning of the pair pivot/jewel bearing (tolerance limits on the whole trial map are +115/-25, +27/+5 and +28/+9 μm for 300, 150 and 100 μm trials, respectively). In this work, the effects of undershoot of the X axis and the uncertainty in the tool center position are the main factors determining the final micro-pin diameter, both severely limiting the application of the present machine in micro precision mechanics.

5.2. R_a

The first conclusion regarding these results is that although the ideal value of $R_a < 0.1$ μm was not reached, the fabricated micro-pins length, due to limitation on the equipment used to measure this value, had an aspect ratio $\frac{L}{D} \approx 13$. However, typical balance staff pivots are very short (with $\frac{L}{D} \sim 2$ [5]) and therefore, better values of R_a, according to the developed hypothesis, should be possible to achieve on micro-pins with $\frac{L}{D}$ of this order of magnitude. Further, looking into the reviewed literature (table 7), a wide range of operating regimes can be applied with satisfactory results. This work appears to be at the extreme end of a_p and f used. While the produced pins can be considered "micro", the optimal operating conditions in this work are orders of magnitude larger than the reviewed micro-turning works (with the exception of [6]). Two effects are important to analyze here. First is the hypothesized relationship between R_a and A_{int}. While this work and [6] have relative large A_{int} (due to high a_p and f) and correspondingly high R_a, works at substantially lower values of these parameters have lower R_a values, which is further evidence to sustain this hypothesis.

Source	R_a (μm)	a_p (μm)	f (μm/rev.)
[7]	$\ll 1$	5	0.012
[8]	0.06	20	0.2
[9]	0.055	75	1
[10] [11]	< 0.1	5	3
[6]	0.33	200	8
This work	0.240	900	10

Table 7: Comparison between this work and reviewed literature: R_a @ optimal a_p and f

Secondly, according to [12], the cutting regime is dependent on the ratio $\frac{f}{r_{edge}}$, where r_{edge} is the *tool cutting edge radius*. While the reviewed works do not present values of r_{edge}, in this work its value was estimated from images taken with a SEM (fig.16) at a value of approximately 5 μm (the manufacturer of the tool used also does not present this value).

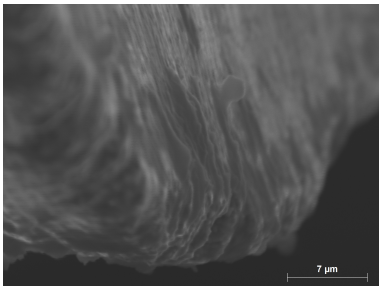

Figure 16: SEM micrograph of the (virgin) turning tool, showing the rounded edge radius

The tool edge radius is evident, with the tool appearing quite blunt at this scale. Based on the best results obtained (f = 5 - 10 μm/rev.), $\frac{f}{r_{edge}} \sim 1 - 2$. From [12], this corresponds to the zone where the cutting mechanism is the concentrated shear deformation of the chip. In this zone, the obtained R_a for brass (R_a = 0.218 μm) is similar to the one obtained in this work. However, the best R_a is achieved only when the cutting mechanism transitions from shear deformation to burnishing ($\frac{f}{r_{edge}}$ = 0.01 - 0.1).

Assuming the reviewed works had $r_{edge} \geq 5$ μm, then works [10], [11], [9] and [8] are likely inside the burnishing range given the low values of f and R_a, much smaller than those obtained in this work (and [6]). This assumption should be valid since: **(i)** tools utilized in these works are either cemented carbide ([10] and [11]) or PCD ([9] and [8]), with the only exception to this being [7], in which a monocrystalline diamond tool is used; **(ii)** although in these works no

grain size is reported for the tool, according to [13], the finest grains for PCD and carbide tools are 0.5 and 0.2 μm, respectively. Since the tool cutting edge must be robust enough to support the cutting forces, it must be made of a large collection of grains, and therefore the cutting edge is only well defined at a scale larger than the grain size. This assumption is not valid for [7], since in principle an atomically sharp and well defined edge can be made on a single crystal. However no definitive value for R_a is presented in this work.

Therefore, the goal of reaching $R_a < 0.1\ \mu m$ should be possible if this work was extended to lower f and a_p values than those tested, to a zone where the effect of vibration and deflection is small and where $\frac{f}{r_{edge}}$ is within the burnishing zone. This is problematic since **(i)** it is currently impossible to achieve lower f given that the developed machine has insufficient resolution and is based on high static/dynamic friction linear guideways; **(ii)** since $D = f(a_p)$, lowering a_p decreases D, which in turn might increase deflection of the micro-pins. A different cutting strategy or a different tool (with lower r_b) need to be used to prevent this.

5.3. Cutting force

With respect to the reviewed works which measured the cutting forces, this work is on the extreme end of experienced cutting forces during micro-turning (refer to table 8). A direct comparison of F_c and k_s can't be established since the specific alloy of brass used in these works is not the same of this thesis.

Source	F_c *(N)*	R_a *(μm)*	f *(μm/rev.)*	k_s $\left(\frac{N}{mm^2}\right)$
[7]	0.013	$\ll 1$	0.012	~ 3000
[10] [11]	~ 1	0.1	3	-
[9]	3.59	0.055	1	-
This work	13.93	0.240	10	1219

Table 8: Comparison between this work and reviewed literature: cutting force at optimal R_a

However, as a general remark, if we define the macro-turning regime as one where the term dU_d is the major contributor to dU_{ext} in eq.12, then this work seems to be positioned below it. According to [14], such macro-turning regime can be bounded near $f \sim 0.5 - 1$ mm/rev. (refer to fig.17) since $k_s \sim 600$ - 500 MPa , which is roughly the same order of magnitude of σ_Y. If we define micro-turning as a regime where the term dU_c is the major contributor to dU_{ext} in eq.12, it might be tempting to describe this work as micro-turning, since the maximum $k_s = 1571$ MPa is around an order of magnitude greater than σ_Y. However, in [7] a value of $\mathbf{k_s}$**= *14000 MPa*** was obtained for extremely low values of f and a_p. Therefore,

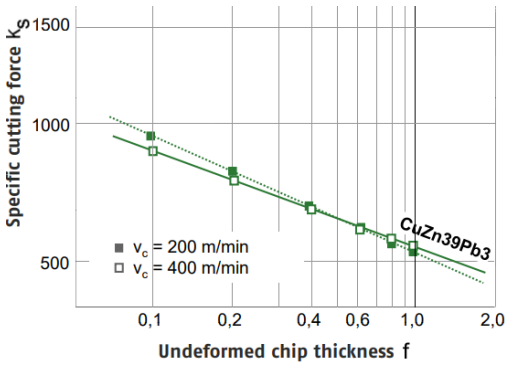

Figure 17: k_s (N/mm^2) vs. f (mm/rev.) (r_b = 0.4 mm and a_p = 1 mm), adapted from [14]

while the fabricated pins were quite small, this work appears to slot well between the micro and macro-turning regimes, with significant contributions from both dU_d and dU_c to dU_{ext}.

References

[1] School, T. W. Illustrated Glossary of Watch Parts `https://www.timezonewatchschool.com/WatchSchool/Glossary/glossary.shtml`.

[2] Baillio, P. Jewel Bearings Solve Light Load Problems, **2020**.

[3] Daniels, G., Watchmaking; Philip Wilson Publishers: A6 Salem Road London W2 4BU, **2014**.

[4] Williams, J. G.; Patel, Y. Fundamentals of cutting. *Interface Focus* **2016**, *6*.

[5] Group, T. SwissNano - Axle `https://youtu.be/D1xwDbUKH6A?t=17`.

[6] Lutfi, M.; Edi, P.; Mamat, A.; Ahmad-Yazid, A. In, **2009**; *76-78*, 532–537.

[7] Lu, Z.; Yoneyama, T. Micro cutting in the micro lathe turning system. *International Journal of Machine Tools and Manufacture* **1999**, *39*, 1171–1183.

[8] Okazaki, Y.; Kitahara, T. Development and Evaluation of a Micro-Lathe Equipped with Numerical Control. *Journal of The Japan Society for Precision Engineering* **2001**, *67*, 1878–1883.

[9] Singh, S.; Ghai, V.; Agrawal, A.; Singh, H. Effect of machining parameters on cutting force during micro-turning of a brass rod. *Materials and Manufacturing Processes* **2019**, *34*, 1816–1823.

[10] Rahman, M.; Kumar, A.; Lim, H. CNC microturning: an application to miniaturization. *International Journal of Machine Tools and Manufacture* **2005**, *45*, 631–639.

[11] Rahman, M.; Kumar, A.; Lim, H. S.; Asad, A. Development of micropin fabrication process using tool based micromachining. *The International Journal of Advanced Manufacturing Technology* **2006**, *27*, 939–944.

[12] Rahman, M. A.; Rahman, M. A.; Kumar, A. P. S.; Amrun, M. R. Effect of cutting edge radius on 'burnishing-like' mechanism in micromachining. *International Journal of Precision Technology* **2018**, *8*, 85.

[13] Sumitool, Insert Grades A1 to A38; Sumitool: **2020**.

[14] At RWTH Aachen University, W., Recommended machining parameters for copper and copper alloys; Deutsches Kupferinstitut: Am Bonneshof 5, 40474 Düsseldorf, Germany, **2010**.